

Direct detection system for independent triplet-sideband signals based on a single photodiode

DONGYAN WU,¹ LEILEI WANG,¹ ZHENG HU,¹ YILIN CHEN,¹ CHENLEI LU,¹ TIANRONG GUO,¹ GEN MIAO,¹ LI ZHAO,²  AND JIANGNAN XIAO^{1,*}

¹University of Shanghai for Science and Technology, Shanghai 200093, China

²School of Information Science and Technology, Fudan University, Shanghai 200433, China

*jiangnanxiao@usst.edu.cn

Received 21 July 2023; revised 12 August 2023; accepted 15 August 2023; posted 17 August 2023; published 12 September 2023

This paper proposes a novel, to the best of our knowledge, independent triplet-single-sideband (triplet-SSB) transmission system scheme aimed at increasing channel capacity and improving spectrum efficiency. The conventional independent multiband transmission systems are limited by their complexity and high computational requirements, which hinder the improvement of spectrum efficiency and channel capacity. To address these challenges, this scheme uses three independent signals, modulated by an in-phase/quadrature (I/Q) modulator, and transmits them over a 5-km standard single-mode fiber (SSMF). At the receiver end, a single photodiode (PD) is used for signal reception, and the signals are separated using digital signal processing (DSP) algorithms. Through simulation and verification, the feasibility and reliability of the system are demonstrated, with the bit error rates (BERs) of all three signals below the hard decision forward error correction (HD-FEC) threshold value of 3.8×10^{-3} . This independent triplet-SSB transmission system scheme effectively improves spectrum efficiency and channel capacity, providing a valuable solution for meeting the growing demands of data transmission. © 2023 Optica Publishing Group

<https://doi.org/10.1364/OL.501255>

With the rapid development of the Internet and mobile communication, there is a continuous increase in demand for high-speed data transmission, making it increasingly important to enhance channel capacity and spectrum efficiency [1–5]. Researchers are conducting research based on the requirements of high spectral efficiency, high channel capacity, low transmission loss, and multi-user transmission. Referring to the literature [6–10], traditional multichannel transmission systems rely heavily on wavelength division multiplexing (WDM) channels. To transmit signals, these channels use multiple external cavity lasers (ECLs), as well as modulators. Following transmission through SSMF, the signal is separated using multiple PDs. However, due to the multitude of components required, such systems are not only structurally complex but also expensive. Then, the independent dual-sideband (dual-SSB) system was developed to simplify the transmission process, replacing the use of multiple

transmitters with two sideband signals: the left sideband (LSB) and the right sideband (RSB). These signals are transmitted and then separated using two optical bandpass filters (OBPFs) [11–15]. Although the dual-SSB system is simpler than the previous transmission method, it still retains a complex structure. Zhao *et al.* proposed a direct detection scheme based on a single PD combined with digital signal processing (DSP) for dual-SSB transmission, reducing the complexity and cost of the receiver [16]. Yu *et al.* conducted the first experimental verification of a single PD dual-SSB detection system without an optical bandpass filter for transmitting two sideband signals over a 10-km single-mode fiber [17]. However, this system is constrained by its capacity to transmit only two independent signals, resulting in suboptimal spectrum efficiency.

Therefore, this paper proposes an independent triplet-SSB signal transmission system based on an in-phase/quadrature (I/Q) modulator, which adds a baseband signal [for unity, this paper calls it a middle sideband (MSB) signal] based on the dual-SSB. The triplet-SSB system has several advantages, including higher spectral efficiency and channel capacity. To implement the triplet-SSB modulation technology, three sideband signals are combined to generate a geometrically shaped 32-quadrature amplitude modulation (GS-32QAM) signal using the beat frequency effect. After SSMF transmission, a PD is used to directly detect the synthesized signal at the receiving end. Finally, a simple DSP algorithm replaces three PDs for signal demodulation and separation.

In this study, the three sideband signals under consideration exhibit low-order QAM modulation. Notably, our investigation reveals that the DAC resolution requirements for synthesizing high-order signals are considerably lower compared to direct import of such signals. The independent triplet-SSB signal scheme is proposed to simulate the superposition of LSB quadrature phase shift keying (QPSK), RSB first quartile QPSK (FQ-QPSK), and MSB binary phase shift keying (BPSK) signals. This includes the transmission of these signals under 1-km and 5-km SSMFs at baud rates of 2 Gbaud and 4 Gbaud. The simulation results demonstrate that it has extraordinarily great error performance.

Figure 1 illustrates the schematic for generating a GS-32QAM signal using three vector signals: LSB, RSB, and MSB. In this

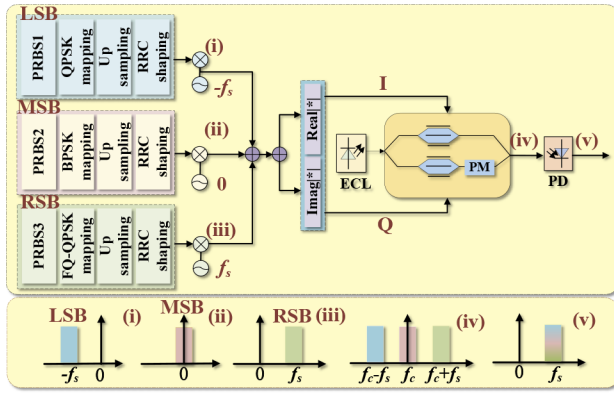


Fig. 1. Schematic for triplet-SSB signal generation. PRBS, pseudo-random binary sequence; RRC, root raised cosine; ECL, external cavity laser; PM, phase modulator; PD, photodiode. (i) Schematic diagram of the LSB signal; (ii) schematic diagram of the MSB signal; (iii) schematic diagram of the RSB signal; (iv) schematic diagram the modulated signal after passing through the I/Q modulator; (v) schematic diagram of the received signal after the PD.

scheme, initially, three low-order QAM sideband signals are formed using pseudo-random binary sequences (PRBSs), then QPSK, FQ-QPSK, and BPSK modulations are carried out on these sideband signals, respectively, through a root-raised cosine (RRC) pulse shaping filter and upconversion, then mixing with the carriers $\exp(-2\pi f_s t)$ and $\exp(2\pi f_s t)$ in a complex sinusoidal form, the frequency modulation on the baseband signal is upconverted to intermediate frequency (IF) signals: LSB, RSB, and MSB. A negative frequency signal represents LSB, a positive frequency denotes RSB, and a frequency of 0 signifies MSB. The three signals can be the same or different in terms of modulation format and carrier rate. Here, the LSB signal is modulated in QPSK format, the RSB signal is modulated in FQ-QPSK format, and the MSB signal is modulated in BPSK format, all at the same carrier rates. Especially, the phase of the two constellation points of MSB BPSK must differ by 90° because of the instability of the baseband signal.

The addition of the three sideband signals will form the driving signal of the I/Q modulator which is denoted by

$$\begin{aligned} E_i(t) &= A(t) \exp(j\varphi_i(t) + j\omega_i(t)) \\ E_r(t) &= B(t) \exp(j\varphi_r(t) + j\omega_r(t)) \\ E_m(t) &= C(t) \exp(j\varphi_m(t) + j\omega_m(t)) \\ E(t) &= E_i(t) + E_r(t) + E_m(t) \end{aligned} \quad (1)$$

where $E_i(t)$, $E_r(t)$, and $E_m(t)$ represent the LSB, RSB and MSB signals, respectively. Here, $A(t)$, $B(t)$, $C(t)$; $\varphi_i(t)$, $\varphi_r(t)$, $\varphi_m(t)$; and $\omega_i(t)$, $\omega_r(t)$, $\omega_m(t)$ denote the amplitudes, phases, and angular frequencies of the LSB, RSB, and MSB signals, respectively. It is divided into real part and imaginary part signals when the signal is input into the IQ modulator at the input end. The real part is also called the in-phase (I) signal, and the imaginary part is also called the quadrature (Q) signal. There is a 90° phase difference between them. The transmission function of the I/Q modulator can be expressed as

$$E_{out}(t) = \frac{1}{2} \cdot E_{in}(t) \cdot [\cos(\frac{\varphi_I(t)}{2}) + j \sin(\frac{\varphi_Q(t)}{2})]. \quad (2)$$

Here, $\varphi_I(t) = \text{Re}[E(t)]/V_\pi \cdot \pi$, $\varphi_Q(t) = \text{Im}[E(t)]/V_\pi \cdot \pi$, where V_π denotes the half-wave voltage of a modulator. Equation (3)

can be deduced by the combination of Eqs. (1) and (2) with the usage of the expansion of Bessel functions. The first three terms of Eq. (3) denote the LSB, RSB, and MSB signals, respectively, and the last term is the carrier term:

$$\begin{aligned} E_{IQ}(t) &= E_{CW} e^{j\omega_c t} [J_1(\alpha) e^{j(\varphi_i + (\omega_c - \omega_s)t)} + \\ &J_1(\beta) e^{j(\varphi_r + (\omega_c + \omega_s)t)} + \\ &J_1(\lambda) e^{j(\varphi_m + \omega_c t)} + J_1(\gamma) e^{j\omega_c t}] \end{aligned} \quad (3)$$

$$\begin{aligned} \alpha &= \pi \cdot A(t)/2V_\pi \\ \beta &= \pi \cdot B(t)/2V_\pi, \\ \lambda &= \pi \cdot C(t)/2V_\pi \end{aligned} \quad (4)$$

where $E_{CW} e^{j\omega_c t}$ is the continuous wave (CW) from the ECL at a frequency of f_c . Here, $J_1(\cdot)$ are the Bessel functions of the first class, γ is a constant related to the extinction ratio (ER), ω_c denotes carrier angular frequency, and ω_s denotes desired sampling angular frequency.

After the optical signal passes PD detection, according to the square law, the photocurrent generated can be expressed as

$$i(t) = \left\{ \begin{aligned} &\frac{1}{2} [J_1^2(\alpha) + J_1^2(\beta) + J_1^2(\lambda) + J_1^2(\gamma)] + \\ &\frac{1}{2} [J_1^2(\alpha) \cos(2(\varphi_i + \omega_c t - \omega_s t)) + \\ &J_1^2(\beta) \cos(2(\varphi_r + \omega_c t + \omega_s t)) + \\ &J_1^2(\lambda) \cos(2(\varphi_m + \omega_c t)) + J_1^2(\gamma) \cos(2\omega_c t)] + \\ &J_1(\alpha)J_1(\beta) [\cos(\varphi_i + \varphi_r + 2\omega_c t) + \cos(\varphi_i - \varphi_r - 2\omega_s t)] + \\ &J_1(\alpha)J_1(\lambda) [\cos(\varphi_i + \varphi_m + 2\omega_c t - \omega_s t) + \cos(\varphi_i - \varphi_m - \omega_s t)] + \\ &J_1(\alpha)J_1(\gamma) [\cos(\varphi_i + 2\omega_c t - \omega_s t) + \cos(\varphi_i - \omega_s t)] + \\ &J_1(\beta)J_1(\lambda) [\cos(\varphi_r + \varphi_m + 2\omega_c t + \omega_s t) + \cos(\varphi_r - \varphi_m + \omega_s t)] + \\ &J_1(\beta)J_1(\gamma) [\cos(\varphi_r + 2\omega_c t + \omega_s t) + \cos(\varphi_r + \omega_s t)] + \\ &J_1(\lambda)J_1(\gamma) [\cos(\varphi_m + 2\omega_c t) + \cos(-\varphi_m)] \end{aligned} \right\}. \quad (5)$$

We can observe that the initial term tends toward the DC component so that it is negligible. Additionally, terms with ω_c need to be omitted, due to the frequency of ω_c being higher than that of PD. Furthermore, the desired signal constructed is located at ω_s , so that the term at $2\omega_s$ can be filtered out. Therefore, Eq. (5) can be approximated as

$$\begin{aligned} i(t) &\approx J_1(\alpha)J_1(\lambda) \cos(\varphi_i - \varphi_m - \omega_s t) + \\ &J_1(\alpha)J_1(\gamma) \cos(\varphi_i - \omega_s t) + \\ &J_1(\beta)J_1(\lambda) \cos(\varphi_r - \varphi_m + \omega_s t) + \\ &J_1(\beta)J_1(\gamma) \cos(\varphi_r + \omega_s t) \end{aligned} \quad (6)$$

Figure 2 depicts the ideal constellations and mapping relationships of signals. The transmitted signal comprises the LSB, RSB, and MSB signals, which are superimposed with rotation and translation to synthesize a GS-32QAM signal. The LSB constellation is represented by four solid dots, namely red, pink, purple, and blue. The RSB constellation also consists of four solid dots, namely yellow, orange, navy, and green. Meanwhile, the MSB signal is composed of two solid points of mixed color. The colors and positions of the miscible points in the different constellations signify the mapping relationship between the transmitted and received signals. Thus, it is possible to demodulate and separate the signals to restore the original signal using DSP algorithms, through their mapping relationships. For instance, the test point in the diagram is composed of a solid purple dot for symbol 1 in the LSB, a solid orange dot for symbol 2 in the RSB, and a solid mixed-color dot for symbol 1 in the MSB,

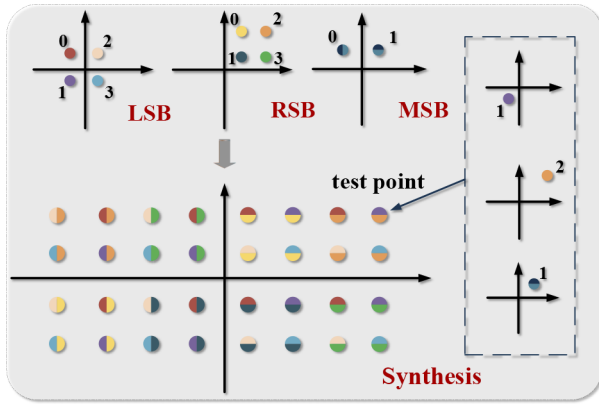


Fig. 2. Ideal constellations and mapping relationship of signals.

Table 1. Symbol Combinations for Signals

GS-32QAM	LSB	RSB	MSB	GS-32QAM	LSB	RSB	MSB
0	3	0	0	16	3	3	1
1	2	0	0	17	1	3	1
2	2	2	0	18	1	2	1
3	3	2	0	19	3	2	1
4	1	0	0	20	2	3	1
5	0	0	0	21	0	3	1
6	0	2	0	22	0	2	1
7	1	2	0	23	2	2	1
8	1	1	0	24	2	1	1
9	0	1	0	25	0	1	1
10	0	3	0	26	0	0	1
11	1	3	0	27	2	0	1
12	3	1	0	28	3	1	1
13	2	1	0	29	1	1	1
14	2	3	0	30	1	0	1
15	3	3	0	31	3	0	1

achieved through rotation and translation. Notably, the left and right halves of the ideal synthetic signal constellation diagram are 90° out of phase due to the 90° phase difference between the two constellation points of the MSB.

The relationship between the amplitude and phase of the GS-32QAM constellation point and those of the LSB, RSB, and MSB constellation points can be described by Eq. (5). The GS-32QAM constellation is represented by a set of symbols including $\{0,1,2,3,4,5,6,7,8,9,10,11,12,13,14,15,16,17,18,19,20,21,22,23,24,25,26,27,28,29,30,31\}$, while the LSB and RSB constellations are denoted by the symbols $\{0,1,2,3\}$, and the MSB constellation is represented by the symbols $\{0,1\}$. The relationship between these constellations is given in Table 1 for reference.

To validate the feasibility and effectiveness of the proposed scheme, simulations are conducted based on IQ modulation. The simulation setup is depicted in Fig. 3 with the key parameters detailed in Table 2. It is worth noting that the externally tunable ECL generates a CW signal with a linewidth of 100 kHz and an emission frequency of 193.1 THz, while the output optical power is 16 dBm. At the transmission end, there are three distinct PRBSs mapped in each of the three sidebands. The data length of all three PRBSs are 2^{14} , while the baud rates are 2 Gbaud and 4 Gbaud, respectively. Initially, three PRBSs are subject to

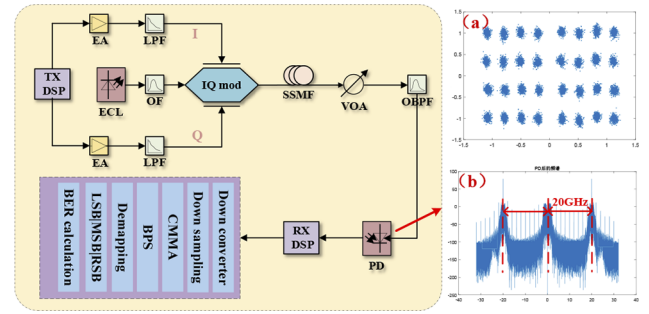


Fig. 3. System simulation diagram of the proposed scheme. EA, electrical amplifier; LPF, low-pass filter; OBPF, optical bandpass filter; SSFM, standard single-mode fiber; VOA, variable optical attenuator. (a) Constellation of GS-32QAM signal; (b) electrical spectrum after PD.

Table 2. Key Parameters in System Simulation

Parameters	Values
DAC sampling rate	64 Gsa/s
ECL average power	16 dBm
ECL linewidth	100 kHz
Vpi DC	2.5 V
Attenuation coefficient	0.2 dB/km
Dispersion	16 ps/nm/km
Nonlinear index	$2.6 \text{ pm}^2/\mu\text{W}$
PD thermal noise	$10 \text{ pA/Hz}^{0.5}$
PD bandwidth	30 GHz

modulation and subsequently mapped into QPSK, FQ-QPSK, and BPSK formats. The modulated signals then undergo upconversion and RRC filtering with a roll-off factor of 0.1. Next, the mixed signals are synthesized through a mixer to generate a GS-32QAM signal, the resulting constellation is shown in Fig. 3(a). Later, the synthetic signal is divided into real and imaginary parts, which are transmitted to the I path and Q path of the IQ modulator, respectively. Specifically, the IQ modulator has a half-wave voltage of 2.5 V, as the modulator operates at the minimum transmission point allows for obtaining a $\pi/2$ phase shift.

After transmitting through the SSFM, the optical signal is passed through a variable optical attenuator (VOA) to achieve precise control over the signal intensity by adjusting the optical power entering the PD. Subsequently, the signal is further processed by an OBPF and detected by a PD. The resulting electrical spectrum is shown in Fig. 3(b), with the synthesized signal at 20 GHz. At the receiving end, a simple DSP algorithm is used to separate and recover the synthesized signal, providing compensation for the non-ideal characteristics of the receiver and significantly reducing its complexity. The key components of the algorithm include a down converter, down sampling, cascaded multi-modulus algorithm (CMMA), blind phase search (BPS), and de-mapping. Ultimately, the evaluation of the restored signal is carried out by calculating the bit error rate (BER) of each individual subband, providing a quantitative assessment of their respective error performance.

Using the aforementioned simulation setup, we investigated the system's transmission performance at different transmission distances and baud rates, and evaluated the feasibility of the proposed scheme based on its error performance. The experimental

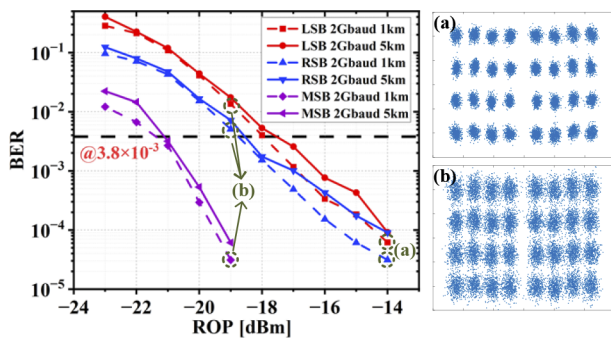


Fig. 4. Relationship between BER and ROP at different SSMFs for a 2-Gbaud baud rate. (a) Constellation diagram at a ROP of -14 dBm; (b) constellation diagram at a ROP of -19 dBm.

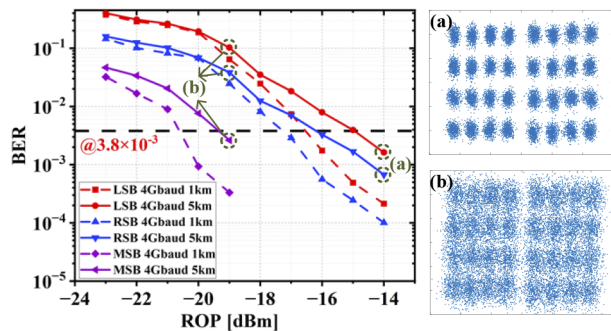


Fig. 5. Relationship between BER and ROP at different SSMFs for a 4-Gbaud baud rate. (a) Constellation diagram at a ROP of -14 dBm; (b) constellation diagram at a ROP of -19 dBm.

results are presented in Figs. 4 and 5, illustrating the relationship between the BER and received optical power (ROP) for the LSB, RSB, and MSB signals under 2-Gbaud and 4-Gbaud baud rates at various transmission distances. Specifically, Figs. 4(a) and 4(b), as well as Figs. 5(a) and 5(b), depict the constellation diagrams at ROP of -14 dBm and -19 dBm. It is evident that as the ROP increases, the constellation diagrams exhibit more clarity. The results indicate that, under 2-Gbaud and 4-Gbaud baud rates and transmission distances of 1 km and 5 km, the BER of each sideband signal remains below the HD-FEC threshold value of 3.8×10^{-3} . Furthermore, it is observed that the BER increases with higher baud rates and longer distances. Additionally, the BER curves of the LSB and RSB signals exhibit similarities, attributed to their comparable modulation formats and power levels. In contrast, the MSB signal consistently demonstrates significantly lower BER in all scenarios, owing not only to differences in modulation format and power levels but also to its baseband positioning that mitigates the dispersion walk-off effect [18]. Conversely, the LSB and RSB signals are susceptible to residual cross talk from the opposing sideband, resulting in increased BER. This observation underscores the impact of dispersion on the transmission quality of digital signals, highlighting the importance of optimizing transmission parameters to ensure reliable communication over short distances.

In this paper, we propose a novel triplet-SSB signal transmission scheme to enhance channel capacity, optimize spectrum

utilization, and minimize multipath effects. This approach builds on the dual-SSB technique by introducing an additional independent signal in the optical carrier, resulting in even better spectrum utilization while maintaining a simple system structure. Furthermore, the triplet-SSB approach reduces system costs and algorithmic complexity by using low-order input signals. At the receiving end, instead of using multiple PDs for signals separation, a DSP algorithm is employed to recover the original signal by demodulation and separation. Specifically, two independent 20-GHz LSB QPSK and RSB FQ-QPSK vector signals, along with an MSB BPSK vector signal in the optical carrier, are used to synthesize the GS-32QAM signal. The performance of the proposed system is evaluated through simulation for SSMF transmission over different distances. Our simulation results show that the BER is lower than the HD-FEC threshold, indicating the feasibility and effectiveness of the scheme. These results demonstrate the promising application prospects of the proposed system in short-distance optical transmission.

Disclosures. The authors declare no conflicts of interest.

Data availability. Data underlying the results presented in this paper are not publicly available at this time but may be obtained from the authors upon reasonable request.

REFERENCES

1. R. Ullah, B. Liu, Q. Zhang, M. Saad Khan, I. Ahmad, A. Ali, R. Khan, Q. Tian, C. Yan, and X. Xin, *Opt. Eng.* **55**, 096106 (2016).
2. W. Zhou and C. Qin, *Opt. Commun.* **398**, 101 (2017).
3. Z. Zhou, J. He, J. Ma, Y. Xiao, and Y. Cheng, *Opt. Fiber Technol.* **48**, 213 (2019).
4. Y. Peng, J. Huang, J. Luo, Z. Yang, L. Wang, X. Wu, X. Zang, C. Yu, M. Gu, Q. Hu, X. Zhang, Y. Zhu, and S. Zhuang, *PhotonIX* **2**, 12 (2021).
5. X. Zang, B. Yao, L. Chen, J. Xie, X. Guo, A. V. Balakin, A. P. Shkurinov, and S. Zhuang, *Light: Adv. Manuf.* **2**, 148 (2021).
6. Z. Dong, H.-C. Chien, J. Yu, J. Zhang, L. Cheng, and G.-K. Chang, *IEEE Photonics Technol. Lett.* **27**, 763 (2015).
7. J. He, H. Dong, R. Deng, J. Shi, and L. Chen, *Opt. Commun.* **374**, 127 (2016).
8. Y. Zhu, X. Zang, H. Chi, Y. Zhou, Y. Zhu, and S. Zhuang, *Light: Adv. Manuf.* **4**, 9 (2023).
9. X. Li, J. Xiao, and J. Yu, *Opt. Express* **22**, 9307 (2014).
10. J. Zhang, J. Yu, F. Li, N. Chi, Z. Dong, and X. Li, *Opt. Express* **21**, 18842 (2013).
11. Y. Wang, W. Zhou, J. Ding, Y. Tan, B. Sang, C. Liu, F. Zhao, and J. Yu, *J. Lightwave Technol.* **39**, 7628 (2021).
12. R. Deng, J. Yu, J. He, M. Chen, Y. Wei, L. Zhao, Q. Zhang, and X. Xin, *J. Lightwave Technol.* **36**, 5562 (2018).
13. X. Pan, X. Liu, H. Zhang, K. Wang, Y. Zhang, D. Ran, X. Wang, and C. Wang, *Opt. Express* **27**, 19906 (2019).
14. H.-C. Chien, Z. Jia, J. Zhang, Z. Dong, and J. Yu, *Opt. Express* **22**, 9465 (2014).
15. Y. Zhu, X. Ruan, K. Zou, and F. Zhang, *J. Lightwave Technol.* **35**, 3629 (2017).
16. L. Zhao, H. Guo, Y. Liu, J. Xiao, T. Wu, S. Song, and L. Guo, *Opt. Express* **30**, 22946 (2022).
17. C. Yu, X. Sheng, R. Gao, F. Wang, Z. Li, H. Chang, L. Huang, Q. Zhang, X. Xin, X. Huang, J. Yan, L. Jiang, S. Cui, L. Kong, and J. Cheng, *Opt. Express* **30**, 37341 (2022).
18. J. Ma, C. Yu, Z. Zhou, and J. Yu, *Opt. Commun.* **268**, 51 (2006).